

## Flatbands under Correlated Perturbations

Joshua D. Bodyfelt,<sup>1</sup> Daniel Leykam,<sup>2</sup> Carlo Danieli,<sup>1</sup> Xiaoquan Yu,<sup>1</sup> and Sergej Flach<sup>1</sup>

<sup>1</sup>*New Zealand Institute for Advanced Study, Centre for Theoretical Chemistry and Physics,  
Massey University, Auckland, 0745 New Zealand*

<sup>2</sup>*Nonlinear Physics Centre, Research School of Physics and Engineering, The Australian National University,  
Canberra, Australian Capital Territory 0200, Australia*

(Received 31 July 2014; published 5 December 2014)

Flatband networks are characterized by the coexistence of dispersive and flatbands. Flatbands (FBs) are generated by compact localized eigenstates (CLSs) with local network symmetries, based on destructive interference. Correlated disorder and quasiperiodic potentials hybridize CLSs without additional renormalization, yet with surprising consequences: (i) states are expelled from the FB energy  $E_{\text{FB}}$ , (ii) the localization length of eigenstates vanishes as  $\xi \sim 1/\ln(E - E_{\text{FB}})$ , (iii) the density of states diverges logarithmically (particle-hole symmetry) and algebraically (no particle-hole symmetry), and (iv) mobility edge curves show algebraic singularities at  $E_{\text{FB}}$ . Our analytical results are based on perturbative expansions of the CLSs and supported by numerical data in one and two lattice dimensions.

DOI: 10.1103/PhysRevLett.113.236403

PACS numbers: 71.23.An, 05.50.+q, 71.30.+h

*Introduction.*—Disorder has a profound effect on waves in periodic potentials, smoothing out van Hove singularities in the density of states and generating Anderson localization [1–3]. Three-dimensional disordered lattices support metal-insulator transitions and mobility edges, while in one and two dimensions the effect of disorder is much simpler, localizing all eigenstates and completely suppressing transport. Correlated disorder changes this picture and allows for complex behavior even in one dimension [4]. Examples include the appearance of resonant transmission channels (random dimer model [5] and tight binding models of DNA [6,7]), metal-insulator transitions (Aubry-André model [8]), and mobility edges (correlations with power-law decay [9,10]). Counterintuitively, certain correlations can even enhance localization [11]. Recent advances have allowed the direct observation of these fundamental effects using cold atoms [12–15] and photonic systems [16–18].

The above elastic potential scattering effects can be both strongly amplified and qualitatively changed when the kinetic energy is quenched, such as in strictly flat dispersion [19–24]. Macroscopically degenerate flatbands occur when perfect destructive interference allows for compact localized eigenstates (CLSs), modes with nonzero amplitude only at a finite number of lattice sites. There are flexible approaches to designing flatband (FB) lattices in a variety of dimensions [14,21,25,26], which can support new topological phases [19] and even model the fractional quantum Hall effect resulting from FB degeneracies of electronic Landau levels interacting within a magnetic field [20].

Anderson localization in flatbands displays a variety of unconventional features including inverse Anderson transitions [25,27], multifractality at weak disorder [28], and effective heavy-tailed disorder distributions [29]. Recently,

the local symmetries of the CLSs were used to detangle uncorrelated disorder into two distinct terms: one that renormalizes the energies of the CLSs and another that hybridizes them with modes belonging to other dispersive bands [30]. This detangling suggests a way to independently control the two terms using appropriately correlated potentials. Such control is feasible with ultracold atoms [12–15] and photonic systems [16–18] but can be also expected for electric or sound propagation along crystal surfaces exposed to adsorbing atoms and molecules.

In this Letter, we consider locally correlated disorder and quasiperiodic potentials in flatband lattices. The compact flatband states hybridize with other dispersive degrees of freedom, but their (bare) energies are not renormalized. This leads to a strong competition between the macroscopic number of compact localized states, generating new spectral singularities (in contrast to uncorrelated disorder, which smooths out all singularities). The resulting surprising action of the perturbations is that (i) all states are expelled from the FB energy  $E_{\text{FB}}$ , (ii) the localization length of eigenstates vanishes as  $\xi \sim 1/\ln(E - E_{\text{FB}})$ , (iii) the density of states diverges logarithmically (particle-hole symmetry) and algebraically (no particle-hole symmetry) for disorder potentials, and (iv) metal-insulator transitions induced by quasiperiodic potentials are promoted by the flatband to mobility edges, whose curves show algebraic singularities at  $E_{\text{FB}}$ . Thus, correlated potentials provide a way to “fine tune” the flatband singularity strength or convert it into more useful form (e.g., mobility edge). Our analytical results are based on perturbative expansions of the CLSs and supported by numerical data.

*One-dimensional model.*—To illustrate the idea, we will start with the simplest case of a one-dimensional (1D) FB model with exactly one dispersive band and one flatband.

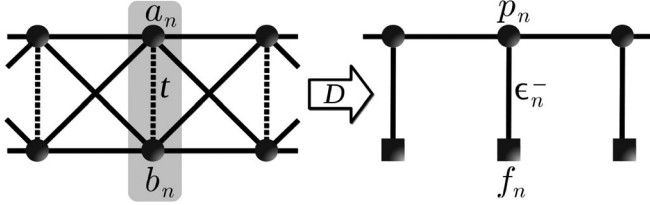


FIG. 1. The cross-stitch lattice structure (left) of Eq. (1). The detangled version of Eq. (3) is shown in the right plot.

The cross-stitch lattice, shown in the left plot in Fig. 1, consists of two interconnected chains. Its unit cell is given by two lattice sites shaded in the figure, and the wave amplitude at the cell is  $\psi_n = (a_n, b_n)^T$ . Stationary waves follow the eigenvalue problem

$$E\psi_n = \epsilon_n\psi_n - tV\psi_n - T(\psi_{n-1} + \psi_{n+1}), \quad (1)$$

with

$$\epsilon_n = \begin{pmatrix} \epsilon_n^a & 0 \\ 0 & \epsilon_n^b \end{pmatrix}, \quad V = \begin{pmatrix} 0 & 1 \\ 1 & 0 \end{pmatrix}, \quad T = \begin{pmatrix} 1 & 1 \\ 1 & 1 \end{pmatrix}.$$

In the crystalline case of  $\epsilon_n = 0$ , Eq. (1) is put into a Bloch basis and diagonalized to give the dispersion curves

$$E(k) = -4 \cos(k) - t, \quad E_{\text{FB}} = t.$$

One band is flat and independent of  $k$ , with Bloch modes  $B_n(k) = (1, -1)^T e^{ikn} / \sqrt{2}$ . Because of the degeneracy, any superposition of these Bloch modes is also an eigenmode, and one can construct compact localized modes  $\psi_n = (1, -1)^T \delta_{n,n_0} / \sqrt{2}$ . Applying the local rotations

$$\phi_n \equiv \begin{pmatrix} p_n \\ f_n \end{pmatrix} = D\psi_n, \quad D = \frac{1}{\sqrt{2}} \begin{pmatrix} 1 & 1 \\ 1 & -1 \end{pmatrix}, \quad (2)$$

with  $\epsilon_n^\pm = (\epsilon_n^a \pm \epsilon_n^b)/2$ , Eq. (1) becomes [30]

$$\begin{aligned} (\bar{E} + 2t)p_n &= \epsilon_n^+ p_n + \epsilon_n^- f_n - 2(p_{n-1} + p_{n+1}), \\ \bar{E}f_n &= \epsilon_n^+ f_n + \epsilon_n^- p_n, \end{aligned} \quad (3)$$

where we measure the energy deviation from  $E_{\text{FB}}$  as  $\bar{E} = E - t$ , and the CLSs  $f_n$  are locally hybridized with the dispersive variables  $p_n$  at strength  $\epsilon_n^-$ , while their energies are renormalized exclusively through nonzero  $\epsilon_n^+$  (see Fig. 1 right). Experimental realizations of the cross-stitch model can be obtained in both its original and detangled forms, the latter having a simpler geometry easily obtained using microwave resonator networks [18].

*Disorder.*—Real systems are never perfect and experience fluctuating deviations from an ideal setup. In Ref. [30], a disorder potential was added assuming that on-site energies  $\epsilon_n^{a,b}$  are random uncorrelated, with a probability density function (PDF) of finite variance

$\mathcal{P}(\epsilon) = 1/W$  for  $|\epsilon| \leq W/2$  and  $\mathcal{P} = 0$  otherwise. Excluding the CLS variables  $f_n$  from Eq. (3), one obtains

$$\frac{\epsilon_n^p - \bar{E}}{2} p_n = p_{n-1} + p_{n+1}, \quad \epsilon_n^p = \epsilon_n^+ + \frac{(\epsilon_n^-)^2}{\bar{E} - \epsilon_n^+} - 2t, \quad (4)$$

which is a tight-binding chain under an energy-dependent on-site disorder potential  $z = \epsilon_n^p$ . Its PDF displays Cauchy tails [30] with diverging variance at the FB energy. Consequently, at weak disorder  $W \ll 1$  the localization length  $\xi$  of an eigenstate  $p_n^v \sim e^{-n/\xi}$  scales as  $\xi \sim 1/W^2$  away from  $E_{\text{FB}}$  and as  $\xi \sim 1/W$  at  $E_{\text{FB}}$ . This energy-dependent inverse localization length  $\xi^{-1}(E)$  is numerically calculated using the recursive iteration

$$\xi^{-1}(E) = \lim_{M \rightarrow +\infty} \frac{1}{M} \sum_{n=1}^M \ln \left| \frac{p_{n+1}}{p_n} \right|. \quad (5)$$

Though the disordered FB states are much more strongly localized than other states, their width still diverges for weak disorder. This is because the disorder is uncorrelated, so it performs both energy renormalization and hybridization with dispersive states at the same time.

A drastic change occurs when the potential is correlated such that energy renormalization no longer occurs, i.e.,  $\epsilon_n^a = -\epsilon_n^b$ , which leads to  $\epsilon_n^+ = 0$  (easily implemented with microwave resonator networks [18]). The remaining potential  $\epsilon_n^-$  has PDF  $\mathcal{P}(\epsilon)$ , and Eq. (4) now displays a Fano resonance at energy  $\bar{E} = 0$  at every lattice site, which strongly scatters the dispersive degree of freedom  $p_n$ . For small  $\bar{E}$ , we can neglect nonresonant terms, and substituting (see the Supplemental Material [31]) into Eq. (5) obtain the localization length

$$\xi^{-1} = \ln \frac{W^2}{8|\bar{E}|} - 2. \quad (6)$$

Hence, irrespective of the strength  $W$  of the correlated disorder, the localization length vanishes due to resonant scattering as the energy tends towards  $E_{\text{FB}}$ . We compute the localization length numerically using Eq. (5). The results in Fig. 2

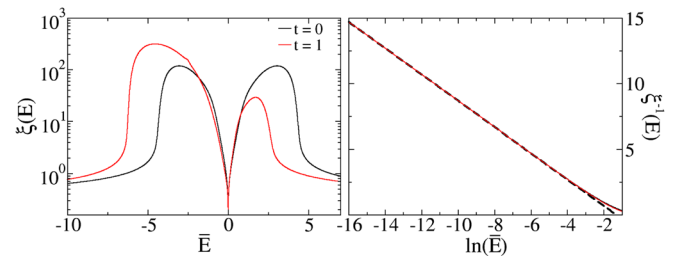


FIG. 2 (color online). Left plot: Localization length  $\xi$  versus eigenstate energy  $\bar{E} = E - t$ , for  $t = 0$  (black solid line) and  $t = 1$  (red solid line). Right plot: Inverse localization length  $\xi^{-1}$  versus  $\ln \bar{E}$  for  $\bar{E} > 0$ , with same color coding as in left plot. The dashed line corresponds to Eq. (6). Here,  $W = 4$ .

(black lines) agree excellently with the analytical predictions (dashed line).

While this picture of a macroscopic number of Fano resonances at  $\bar{E} = 0$  can intuitively explain the behavior of the localization length, surprisingly, the flatband energy  $E_{\text{FB}}$  is completely emptied: no eigenstate can reside there. This follows directly from Eq. (3), which now allows only for a trivial solution  $p_n = f_n = 0$  when  $E = E_{\text{FB}} = t$ . All the compact localized states have hybridized and shifted their energies away; however, a significant fraction stay energetically close to  $E_{\text{FB}}$ , such that the density of states still diverges at  $E_{\text{FB}}$ . To show this, we note that close to resonance the eigenmodes should strongly excite the CLSs, which may hybridize among themselves. The weak energy shifts of these states imply the existence of a small parameter, which can be used for perturbative calculations. We consider first  $t = 0$ . Up to normalization, we construct (Supplemental Material [31]) dimerlike states at energy  $\bar{E} = \pm(\epsilon_0^- \epsilon_1^-)/2 \ll W^2/4$  (position shifts can be done without loss of generality) as  $f_0 = f_1 = \pm 1$ ,  $p_0 = \pm \epsilon_1^-/2$ ,  $p_1 = \epsilon_0^-/2$ ,  $p_{n \geq 2} = \pm \epsilon_0^- (2\bar{E})^{n-1} / (\prod_{m=2}^n \epsilon_m^-)^2$ ,  $f_{n \geq 2} = \pm 2p_{n-1}/\epsilon_n^-$ .

The density of states  $\rho(\bar{E})$  for small  $\bar{E}$  follows (Supplemental Material [31]) from the PDF  $\int_{-\infty}^{+\infty} \mathcal{P}(x)\mathcal{P}(z/x)|x|^{-1} dx$  of the random number  $z = \epsilon_0 \epsilon_1$  as

$$\rho(\bar{E}) = \frac{4}{W^2} \left( \ln \frac{W}{2} - \ln \frac{4|\bar{E}|}{W} \right). \quad (7)$$

Despite the result that eigenstates strictly do not exist at  $E_{\text{FB}}$ , the density of states  $\rho(\bar{E})$  diverges logarithmically at  $E_{\text{FB}}$ .

We perform diagonalizations of Eq. (1) and obtain the density of states following well-known schemes (see Chap. 3 in Ref. [32]). The result in the left of Fig. 3 confirms the predicted logarithmic divergence. It therefore also confirms that we identified the correct group of eigenstates responsible for the divergence.

When the FB energy is shifted away from the particle-hole symmetry point  $E_{\text{FB}} = t \neq 0$ , the nature of the localized states changes. At the energy  $\bar{E} = \epsilon_0^2/(2t)$ , we

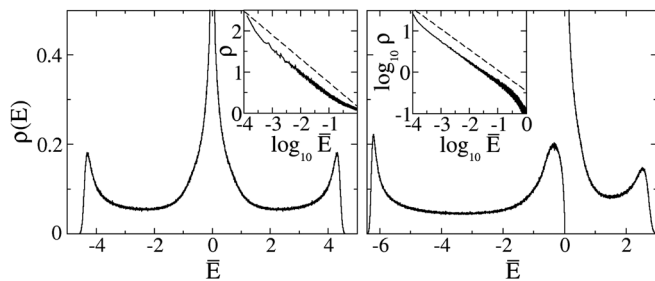


FIG. 3. Density of states  $\rho(\bar{E})$  for  $t = 0$  (left) and  $t = 1$  (right). Divergences are observed at the flatband energies  $\bar{E} = 0$ . Logarithmic scalings of positive  $\bar{E}$  in the insets describe the divergent behavior, and the dashed lines indicate theoretical results of Eqs. (7) and (8). Here,  $W = 4$ .

obtain (Supplemental Material [31]) states with  $f_0 = 1$ ,  $p_0 = \epsilon_0/(2t)$ ,  $p_{n \geq 1} = p_0 (2\bar{E})^n / (\prod_{m=1}^n \epsilon_m)^2$ ,  $f_{n \geq 1} = 2p_{n-1}/\epsilon_n$ . The dimers are destroyed, leaving single-peaked resonant states. While the localization length of these states follows the  $t = 0$  case of Eq. (6) (Fig. 2 red curves), the density of states behaves quite differently. First, we note that the obtained states have positive  $\bar{E}$ , which means that they must occur on the larger energy side of the FB energy. Furthermore, the density of states  $\rho(E)$  follows (Supplemental Material [31]) from the PDF  $f(z) = 1/(W\sqrt{z})$  of the random number  $z = \epsilon_0^2$  as

$$\rho(\bar{E}) = \frac{1}{W} \sqrt{\frac{2t}{\bar{E}}}. \quad (8)$$

The divergence is now strengthened to a square root one, but only on the high-energy side of the FB energy. In Fig. 3, we indeed confirm this singularity numerically on the right-hand side of the FB energy. Meanwhile, on the left-hand side, we instead observe a vanishing density of states. It should be also noted that we observe a gap developing as  $t$  increases beyond a critical  $t_c$  [33]. This issue warrants further investigation and may be related to disorder-induced crossing resonances [34].

**Mobility edges.**—Since the localization length is forced to vanish at the FB energy by correlated disorder in a one-dimensional system, it can be expected that a system with a metal-insulator transition will even have a singularity in the mobility edge, i.e., the dependence of the critical potential strength on the eigenstate energy. Mobility edges typically appear for three-dimensional disordered systems; however, a quasiperiodic potential is known to produce a metal-insulator transition already in one space dimension. Indeed, a tight-binding chain with eigenvalue problem  $E\phi_n = \lambda \cos(2\pi\alpha n + \beta)\phi_n - (\phi_{n+1} + \phi_{n-1})$  is the well-known Aubry-André model that has a metal-insulator transition at  $\lambda_c = 2$ , provided  $\alpha$  is an irrational number [8]. Note that  $\lambda_c$  does not depend on the eigenenergy; therefore, the mobility edge function is a constant in the Aubry-André case. In general, deviations from the Aubry-André quasiperiodic case into other quasiperiodic potentials will lead to the appearance of mobility edges [35–38]; however, here we engineer them via a predictable analytical expression.

We again consider a correlated, quasiperiodic potential  $\epsilon_n^a = -\epsilon_n^b = \lambda \cos(2\pi\alpha n)$ . Equation (4) can be rewritten as

$$\tilde{E}p_n = \tilde{\lambda} \cos(4\pi\alpha n)p_n - (p_{n-1} + p_{n+1}), \quad (9)$$

where

$$\tilde{\lambda} = \frac{\lambda^2}{4(E-t)}, \quad \tilde{E} := \frac{E+t}{2} - \frac{\lambda^2}{4(E-t)}. \quad (10)$$

Equation (9) takes the form of a regular Aubry-André model; however, with effective energy  $\tilde{E}$  and potential strength  $\tilde{\lambda}$ , which are functions of the eigenstate energy

$E$  and the original potential strength  $\lambda$ , i.e., Eq. (10). Therefore, if present, a metal-insulator transition must occur for  $\tilde{\lambda} = 2$ . This immediately yields a mobility edge dependence  $\lambda_c(E)$ ,

$$\left| \frac{\lambda_c^2}{4(E-t)} \right| = 2 \Rightarrow \lambda_c(E) = 2\sqrt{2|E-t|}. \quad (11)$$

For  $E = t$ , the mobility edge curve is singular and zero, corresponding to the lack of any states, as previously mentioned. In Fig. 4 we show the spectrum of Eq. (9) as a function of  $\lambda$ . We again compute the localization length  $\xi(E, \lambda)$  with Eq. (5). If the recursion converges to a finite number (localized states, insulator), we plot blue points, while diverging cases are plotted in red (extended states, metal). The theoretical prediction Eq. (11) is also plotted and shows excellent agreement with numerical data.

*Generalizations.*—Remarkably, this construction works in a plethora of other flatband models with CLSs. In higher dimensional lattices, the construction of low-energy eigenstates can proceed in exactly the same way: because the localization length is forced to vanish, for sufficiently small  $\tilde{E}$  the eigenstates are near sighted, so their properties are insensitive to the lattice dimension. The divergence in the density of states persists, in contrast to the more familiar van Hove singularities that get weaker as the dimension increases.

As an example, we consider the two-dimensional (2D) Lieb lattice, which hosts a flatband with nontrivial topology. Here, the compact localized states occupy multiple unit cells (shaded in Fig. 5) and form an overcomplete nonorthogonal basis. Furthermore, the flatband is frustrated: its projector is long ranged (power-law decay in real space) and it is forced to touch another dispersive band [24,28,39]. The band structure is determined by two dispersive  $E_{\pm}$  and one flatband  $E_{\text{FB}}$  [40] (here all hoppings are assumed to be of value unity)

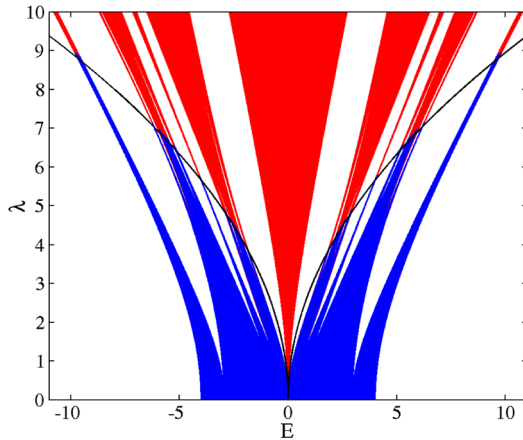


FIG. 4 (color online). Spectrum of an  $N = 512$  unit cell chain under antisymmetric quasiperiodic perturbation with strength  $\lambda$ . The analytically predicted mobility edge Eq. (11) (black line) separates extended (blue) and localized (red;  $\xi < 51$ ) modes.

$$E_{\pm}(k_x, k_y) = \pm 2\sqrt{\cos^2 \frac{k_x}{2} + \cos^2 \frac{k_y}{2}}, \quad E_{\text{FB}} = 0. \quad (12)$$

For a given CLS, any on-site potential can be represented as a sum of a CLS-preserving part and its orthogonal counterpart. A correlated potential for that given CLS is then defined by zeroing the CLS-preserving part. Because of the above mentioned nontrivial topology of the 2D Lieb lattice, this procedure can be extended to every second CLS in a checkerboard arrangement with unit cell coordinates  $l_x = m + n$  and  $l_y = m - n$  ( $m, n$  are integers). We realize the correlated potential by choosing  $\epsilon_{2j} = (-1)^j \delta$  in each eight-site plaquette of a participating CLS (dashed enclosure) in Fig. 5(a) ( $\delta$  and the on-site energies  $\epsilon_{2j-1}$  in the plaquette are random uncorrelated numbers with PDF  $\mathcal{P}$ ). Similar to the cross-stitch example, there are rapidly decaying eigenmodes with  $E \sim \delta^2 \ll W^2/2$ , which yield a square root singularity in the density of states. Figure 5(c) shows the corresponding numerical results [41]. The predicted square root singularity at  $E = 0$  lies on top of a background of width  $W$  formed by the remaining CLSs that have their energies renormalized. Also visible are two peaks at  $E = \pm 2$ , which are the van Hove singularities that have been regularized by the disorder. We note that the Lieb lattice was very recently fabricated as a photonic lattice using femtosecond laser writing [42,43]. The required correlations can be readily introduced by modulation of the waveguide depths.

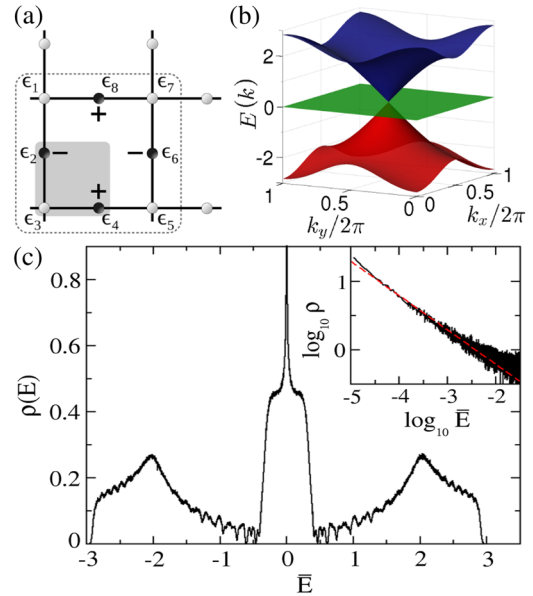


FIG. 5 (color online). (a) The 2D Lieb lattice: its unit cell (shaded region), the eight-site plaquette (dashed enclosure), and the minimal compact state (black circles). (b) The band structure  $E(k_x, k_y)$  from Eq. (12). Red  $E_-$  (bottom) and blue  $E_+$  (top) bands are dispersive, and the central  $E_{\text{FB}}$  (green) band is flat. (c) Density of states under the correlation  $\epsilon_{2j} = (-1)^j \epsilon_a$  enforced at each plaquette, displaying square root singularity at  $E = 0$ ;  $W = 1$ . Lattice size is  $N = 24 \times 24$  unit cells [44]. The red line is a linear fit.

*Conclusion.*—We have shown how appropriately correlated disorder can transform the singular density of states at a flatband into weaker logarithmic or square root divergences. The resulting simple, analytically tractable models feature vanishing localization lengths for arbitrarily weak disorder and mobility edges for quasiperiodic perturbations. This approach offers a flexible and intuitive way to engineer different types of spectral singularities or mobility edges in lattice systems and control wave transport.

### ACKNOWLEDGMENTS

The authors wish to thank J. Richter for motivating discussions. D.L. acknowledges funding from the Australian Research Council.

- 
- [1] L. Van Hove, *Phys. Rev.* **89**, 1189 (1953).  
 [2] P. W. Anderson, *Phys. Rev.* **109**, 1492 (1958).  
 [3] B. Kramer and A. MacKinnon, *Rep. Prog. Phys.* **56**, 1469 (1993).  
 [4] F. M. Izrailev, A. A. Krokhin, and N. M. Makarov, *Phys. Rep.* **512**, 125 (2012).  
 [5] D. H. Dunlap, H. L. Wu, and P. W. Phillips, *Phys. Rev. Lett.* **65**, 88 (1990).  
 [6] D. Klotsa, R. A. Römer, and M. S. Turner, *Biophys. J.* **89**, 2187 (2005).  
 [7] A. A. Krokhin, V. M. K. Bagci, F. M. Izrailev, O. V. Usatenko, and V. A. Yampol'skii, *Phys. Rev. B* **80**, 085420 (2009).  
 [8] S. Aubry and G. Andre, *Ann. Isr. Phys. Soc.* **3**, 133 (1980).  
 [9] F. A. B. F. de Moura and M. L. Lyra, *Phys. Rev. Lett.* **81**, 3735 (1998).  
 [10] F. M. Izrailev and A. A. Krokhin, *Phys. Rev. Lett.* **82**, 4062 (1999).  
 [11] U. Kuhl, F. M. Izrailev, and A. A. Krokhin, *Phys. Rev. Lett.* **100**, 126402 (2008).  
 [12] J. Billy, V. Josse, Z. Zuo, A. Bernard, B. Hambrecht, P. Lugan, D. Clément, L. Sanchez-Palencia, P. Bouyer, and A. Aspect, *Nature (London)* **453**, 891 (2008); G. Roati, C. D'Errico, L. Fallani, M. Fattori, C. Fort, M. Zaccanti, G. Modugno, M. Modugno, and M. Inguscio, *ibid.* **453**, 895 (2008).  
 [13] C. Wu, D. Bergman, L. Balents, and S. Das Sarma, *Phys. Rev. Lett.* **99**, 070401 (2007).  
 [14] M. Hyrkäs, V. Apaja, and M. Manninen, *Phys. Rev. A* **87**, 023614 (2013).  
 [15] L. Sanchez-Palencia and M. Lewenstein, *Nat. Phys.* **6**, 87 (2010).  
 [16] U. Kuhl, F. M. Izrailev, A. A. Krokhin, and H.-J. Stöckmann, *Appl. Phys. Lett.* **77**, 633 (2000).  
 [17] O. Dietz, U. Kuhl, H.-J. Stöckmann, N. M. Makarov, and F. M. Izrailev, *Phys. Rev. B* **83**, 134203 (2011).  
 [18] M. Bellec, U. Kuhl, G. Montambaux, and F. Mortessagne, *Phys. Rev. B* **88**, 115437 (2013).  
 [19] E. J. Bergholtz and Z. Lu, *Int. J. Mod. Phys. B* **27**, 1330017 (2013).  
 [20] A. Parameswaran, R. Roy, and S. L. Sondhi, *C.R. Phys.* **14**, 816 (2013).  
 [21] O. Derzhko and J. Richter, *Eur. Phys. J. B* **52**, 23 (2006); O. Derzhko, J. Richter, A. Honecker, M. Maksymenko, and R. Moessner, *Phys. Rev. B* **81**, 014421 (2010).  
 [22] A. Mielke, *J. Phys. A* **24**, L73 (1991); **24**, 3311 (1991); **25**, 4335 (1992).  
 [23] H. Tasaki, *Phys. Rev. Lett.* **69**, 1608 (1992).  
 [24] D. L. Bergman, C. Wu, and L. Balents, *Phys. Rev. B* **78**, 125104 (2008).  
 [25] M. Goda, S. Nishino, and H. Matsuda, *Phys. Rev. Lett.* **96**, 126401 (2006).  
 [26] S. D. Huber and E. Altman, *Phys. Rev. B* **82**, 184502 (2010); D. Green, L. Santos, and C. Chamon, *Phys. Rev. B* **82**, 075104 (2010).  
 [27] S. Nishino, H. Matsuda, and M. Goda, *J. Phys. Soc. Jpn.* **76**, 024709 (2007).  
 [28] J. T. Chalker, T. S. Pickles, and P. Shukla, *Phys. Rev. B* **82**, 104209 (2010).  
 [29] D. Leykam, S. Flach, O. Bahat-Treidel, and A. S. Desyatnikov, *Phys. Rev. B* **88**, 224203 (2013).  
 [30] S. Flach, D. Leykam, J. D. Bodyfelt, P. Matthies, and A. S. Desyatnikov, *Europhys. Lett.* **105**, 30001 (2014); **106**, 19901 (2014).  
 [31] See the Supplemental Material at <http://link.aps.org/supplemental/10.1103/PhysRevLett.113.236403> for the low-energy derivations of Eqs. (6)–(8) and their corresponding eigenstates.  
 [32] H.-J. Stöckmann, *Quantum Chaos* (Cambridge University Press, Cambridge, England, 2006).  
 [33] The value observed is  $t_c > 1$ ; however, in such a gap we see no indication of Lifshitz-Urbach tails signifying rare states. Since our understanding is based solely on numerics, we can not completely exclude these rare events, and therefore can not provide an exact value to  $t_c$ . Further investigation into gap development is ongoing.  
 [34] V. A. Ignatchenko and D. S. Polukhin, *JETP* **116**, 206 (2013); **117**, 846 (2013).  
 [35] C. M. Soukoulis and E. N. Economou, *Phys. Rev. Lett.* **48**, 1043 (1982).  
 [36] H. Hiramoto and M. Kohmoto, *Phys. Rev. B* **40**, 8225 (1989).  
 [37] P. Zhou, X. Fu, Z. Guo, and Y. Liu, *Solid State Commun.* **96**, 373 (1995).  
 [38] G. Ananthakrishna, H. Zewdie, P. K. Thakur, and F. Brouers, *Prog. Cryst. Growth Charact.* **34**, 133 (1997).  
 [39] A. A. Lopes and R. G. Dias, *Phys. Rev. B* **84**, 085124 (2011).  
 [40] M. Nita, B. Ostahie, and A. Aldea, *Phys. Rev. B* **87**, 125428 (2013).  
 [41] There is no gap in this case: disorder breaks the particle-hole symmetry, but the ensemble average restores it.  
 [42] D. Guzmán-Silva, C. Meijá-Cortés, M. A. Bandres, M. C. Rechtsman, S. Weimann, S. Nolte, M. Segev, A. Szameit, and R. A. Vicencio, *New J. Phys.* **16**, 063061 (2014).  
 [43] F. Diebel, D. Leykam, S. Kroesen, C. Denz, and A. S. Desyatnikov, in *Advanced Photonics*, OSA Technical Digest (online) (Optical Society of America, Washington, DC, 2014), paper NW3A.1.  
 [44] Because  $\xi \rightarrow 0$  at  $E_{FB}$ , this is sufficient to avoid finite size effects. We checked that increasing the lattice size does not significantly change the results.